Available online at www.sciencedirect.com

SCIENCE DIRECT®

Remote Sensing of Environment 94 (2005) 105–122

Remote Sensing of Environment

www.elsevier.com/locate/rse

Satellite-based modeling of gross primary production in a seasonally moist tropical evergreen forest

Xiangming Xiao[a,*], Qingyuan Zhang[a], Scott Saleska[b], Lucy Hutyra[b], Plinio De Camargo[c], Steven Wofsy[b], Stephen Frolking[a], Stephen Boles[a], Michael Keller[a,d], Berrien Moore III[a]

[a]*Institute for the Study of Earth, Oceans and Space, University of New Hampshire, Durham, NH 03824, USA*
[b]*Department of Earth and Planetary Sciences, Harvard University, Cambridge, MA 02138, USA*
[c]*Centro de Energia Nuclear na Agricultura (CENA), Universidade de São Paulo, Brazil*
[d]*USDA Forest Service, International Institute of Tropical Forestry, San Juan, Puerto Rico, 00926, USA*

Received 16 April 2004; received in revised form 26 August 2004; accepted 29 August 2004

Abstract

A CO_2 eddy flux tower study has recently reported that an old-growth stand of seasonally moist tropical evergreen forest in Santarém, Brazil, maintained high gross primary production (GPP) during the dry seasons [Saleska, S. R., Miller, S. D., Matross, D. M., Goulden, M. L., Wofsy, S. C., da Rocha, H. R., de Camargo, P. B., Crill, P., Daube, B. C., de Freitas, H. C., Hutyra, L., Keller, M., Kirchhoff, V., Menton, M., Munger, J. W., Pyle, E. H., Rice, A. H., & Silva, H. (2003). Carbon in amazon forests: Unexpected seasonal fluxes and disturbance-induced losses. *Science*, *302*, 1554–1557]. It was proposed that seasonally moist tropical evergreen forests have evolved two adaptive mechanisms in an environment with strong seasonal variations of light and water: deep roots system for access to water in deep soils and leaf phenology for access to light. Identifying tropical forests with these adaptive mechanisms could substantially improve our capacity of modeling the seasonal dynamics of carbon and water fluxes in the tropical zone. In this paper, we have analyzed multi-year satellite images from the VEGETATION (VGT) sensor onboard the SPOT-4 satellite (4/1998–12/2002) and the Moderate Resolution Imaging Spectroradiometer (MODIS) onboard the Terra satellite (2000–2003). We reported temporal analyses of vegetation indices and simulations of the satellite-based vegetation photosynthesis model (VPM). The Enhanced Vegetation Index (EVI) identified subtle changes in the seasonal dynamics of leaf phenology (leaf emergence, leaf aging and leaf fall) in the forest, as suggested by the leaf litterfall data. The land surface water index (LSWI) indicated that the forest experienced no water stress in the dry seasons of 1998–2002. The VPM model, which uses EVI, LSWI and site-specific climate data (air temperature and photosynthetically active radiation, PAR) for 2001–2002, predicted high GPP in the late dry seasons, consistent with observed high evapotranspiration and estimated GPP from the CO_2 eddy flux tower.

Keywords: Leaf phenology; Vegetation index; Liquid water index; Vegetation photosynthesis model

1. Introduction

Seasonally moist tropical forests in the Amazon basin have high annual precipitation with distinct wet and dry seasons. There is a strong seasonality of photosynthetically active radiation (PAR), usually being much larger in the dry season than in the wet season. Field studies at individual sites in the Amazon region have shown that seasonally moist tropical forests maintain high gross and net primary production (GPP and NPP) throughout dry seasons that extend up to 5–6 months (Nepstad et al., 1994; Saleska et al., 2003). The seasonally moist tropical forests may have evolved two adaptive mechanisms to maximize carbon uptake in an environment with large seasonal variations of light and water. One adaptive mechanism is that many

* Corresponding author. Institute for the Study of Earth, Oceans and Space, University of New Hampshire, Durham, NH 03833, USA. Tel.: +1 603 8623818; fax: +1 603 862 0188.
E-mail address: xiangming.xiao@unh.edu (X. Xiao).

0034-4257/$ - see front matter © 2004 Elsevier Inc. All rights reserved.
doi:10.1016/j.rse.2004.08.015

plants in the tropical forest have deep roots (10-m and deeper) for getting access to water in deep soils during the dry season (Nepstad et al., 1994). For the dense forest at the Tapajos National Forest in Brazil, dry season evapotranspiration was ~4.0 mm/day while wet–season evapotranspiration was ~3.2 mm/day (da Rocha et al., in press). The second adaptive mechanism may be the leaf phenology (seasonal dynamics of leaf fall and leaf emergence). Field observations have shown that seasonally moist tropical evergreen forests in the Amazon basin have distinct seasonal dynamics of litterfall, with a peak litterfall rate during the dry season (Luizao, 1989) and dry-season flushing of new leaves (Sarmiento et al., 1985; Van Schaik et al., 1993; Wright & van Schaik, 1994).

In this study, we combined analyses of satellite images with field data from a CO_2 flux tower site of seasonally moist tropical evergreen forest in Brazil (Saleska et al., 2003). The objective of this study was to develop and validate a new satellite-based vegetation photosynthesis model (VPM) for estimating seasonal dynamics of GPP in a seasonally moist tropical evergreen forest. The VPM model (Xiao et al., 2004a,b) takes advantages of additional spectral bands (e.g., blue and shortwave infrared (SWIR)) that are available from advanced optical sensors. This new generation of optical sensors includes VEGETATION (VGT) sensor onboard the SPOT-4 satellite, and the Moderate Resolution Imaging Spectroradiometer (MODIS) onboard the NASA Terra and Aqua satellites, both of which offer the potential for improved characterization of vegetation at the global scale. The input data to the VPM model are the enhanced vegetation index (EVI; Huete et al., 1997), the land surface water index (LSWI; (Xiao et al., 2004a)), air temperature, and PAR.

Over the last few decades, the time-series data of the normalized difference vegetation index (NDVI), which is calculated as the normalized ratio between red and near-infrared (NIR) bands, have been widely used in satellite-based modeling of GPP and NPP of terrestrial vegetation (Field et al., 1995; Nemani et al., 2003; Potter et al., 1993; Prince & Goward, 1995). The advanced very high resolution radiometer (AVHRR) sensors that have red and near-infrared (NIR) bands have provided multi-decadal time series of NDVI data for the globe. However, it is well known that NDVI has several limitations, including saturation in a multilayer closed canopy and sensitivity to both atmospheric aerosols and the soil background (Huete et al., 2002; Xiao et al., 2003). To account for these limitations of NDVI, the enhanced vegetation index (EVI) was developed (Huete et al., 1997).

$$\mathrm{NDVI} = \frac{\rho_{\mathrm{nir}} - \rho_{\mathrm{red}}}{\rho_{\mathrm{nir}} + \rho_{\mathrm{red}}} \tag{1}$$

$$\mathrm{EVI} = 2.5 \times \frac{\rho_{\mathrm{nir}} - \rho_{\mathrm{red}}}{\rho_{\mathrm{nir}} + (6 \times \rho_{\mathrm{red}} - 7.5 \times \rho_{\mathrm{blue}}) + 1}. \tag{2}$$

EVI includes the blue band for atmospheric correction, which is one important feature for the study in the Amazon basin where seasonal burning of pasture and forest takes place throughout the dry season, either for agricultural purpose (land clearing) or natural fire events. The smoke and aerosols from the biomass burning could affect NDVI substantially, irrespective of vegetation changes. The advanced optical sensors (VGT and MODIS) have additional spectral bands (e.g., blue and shortwave infrared), making it possible to develop time-series data of improved vegetation indices. EVI has recently been used for the study of temperate forests (Boles et al., 2004; Xiao et al., 2004a; Zhang et al., 2003), and is much less sensitive to aerosols (from biomass burning) than is NDVI (Xiao et al., 2003).

As the short infrared (SWIR) spectral band is sensitive to vegetation water content and soil moisture, a combination of NIR and SWIR bands have been used to derive water-sensitive vegetation indices (Ceccato et al., 2001, 2002a,b; Xiao et al., 2004a), including the land surface water index (LSWI; Boles et al., 2004; Xiao et al., 2002, 2004a).

$$\mathrm{LSWI} = \frac{\rho_{\mathrm{nir}} - \rho_{\mathrm{swir}}}{\rho_{\mathrm{nir}} + \rho_{\mathrm{swir}}}. \tag{3}$$

As leaf liquid water content increases or soil moisture increases, SWIR absorption increases and SWIR reflectance decreases, resulting in an increase of LSWI value. Recent work in evergreen needleleaf forests have shown that LSWI is sensitive to changes in leaf water content (equivalent water thickness (EWT), g H_2O/m^2) over time (Maki et al., 2004; Xiao et al., 2004a).

2. Brief description of the vegetation photosynthesis model (VPM)

2.1. Overview of the VPM model

Leaves and canopy are composed of photosynthetically active vegetation (PAV; chloroplasts) and non-photosynthetic vegetation (NPV; e.g., stem, branch, cell wall, vein). Based on the conceptual partitioning of PAV and NPV, the VPM model was recently developed to estimate GPP of forests (Xiao et al., 2004a,b). Here we give a brief description of the VPM model:

$$\mathrm{GPP} = \varepsilon_g \times \mathrm{FAPAR}_{\mathrm{PAV}} \times \mathrm{PAR} \tag{4}$$

$$\varepsilon_g = \varepsilon_0 \times T_{\mathrm{scalar}} \times W_{\mathrm{scalar}} \times P_{\mathrm{scalar}} \tag{5}$$

where PAR is the photosynthetically active radiation (μmol/m^2/s, photosynthetic photon flux density, PPFD), $\mathrm{FAPAR}_{\mathrm{PAV}}$ is the fraction of PAR absorbed by PAV (chloroplasts), ε_g is the light use efficiency (μmol CO_2/μmol mol PAR). The parameter ε_0 is the apparent quantum yield or maximum light use efficiency (μmol CO_2 /μmol PAR), and T_{scalar}, W_{scalar} and P_{scalar} are the down-regulation scalars for the effects of temperature, water and leaf phenology on the light use efficiency of vegetation, respectively.

In the current version of the VPM model, $FAPAR_{PAV}$ is assumed to be a linear function of EVI, and the coefficient a in Eq. (6) is simply set to be 1.0 (Xiao et al., 2004a,b):

$$FAPAR_{PAV} = a \times EVI \quad (6)$$

T_{scalar} is estimated at each time step, using the equation developed for the Terrestrial Ecosystem Model (Raich et al., 1991):

$$T_{scalar} = \frac{(T - T_{min})(T - T_{max})}{[(T - T_{min})(T - T_{max})] - (T - T_{opt})^2} \quad (7)$$

where T_{min}, T_{max} and T_{opt} are minimum, maximum and optimal temperature for photosynthetic activities, respectively. If air temperature falls below T_{min}, T_{scalar} is set to be zero.

W_{scalar}, the effect of water on plant photosynthesis, has been estimated as a function of soil moisture and/or vapor pressure deficit (VPD) in a number of Production Efficiency Models (Field et al., 1995; Prince & Goward, 1995; Running et al., 2000). As the first order of approximation, we proposed an alternative and simple approach that uses a satellite-derived water index to estimate the seasonal dynamics of W_{scalar} (Xiao et al., 2004a,b).

$$W_{scalar} = \frac{1 + LSWI}{1 + LSWI_{max}} \quad (8)$$

where $LSWI_{max}$ is the maximum LSWI within the plant-growing season for individual pixels.

P_{scalar} is included to account for the effect of leaf phenology (leaf age) on photosynthesis at the canopy level. In this version of the VPM model, calculation of P_{scalar} is dependent upon the longevity of leaves (deciduous, versus evergreen). For a canopy that is dominated by leaves with a life expectancy of 1 year (one growing season, e.g., deciduous trees), P_{scalar} is calculated at two different phases as a linear function (Xiao et al., 2004b):

$$P_{scalar} = \frac{1 + LSWI}{2} \quad (9)$$

During bud burst to leaf full expansion

$$P_{scalar} = 1 \quad \text{After leaf full expansion} \quad (10)$$

LSWI values range from −1 to +1 (a range of 2), and the simplest formulation of P_{scalar} (Eq. (9)) is a linear scalar with a value range of 0 to 1. Evergreen broadleaf trees in the tropical zone have a green canopy throughout the year because foliage is retained for several growing seasons. Canopies of evergreen broadleaf forests are thus composed of green leaves of various ages. In this version of the VPM model, a simple assumption of P_{scalar} is made for evergreen broadleaf forests, similar to the assumption we used for evergreen needleleaf forests (Xiao et al., 2004a):

$$P_{scalar} = 1 \quad (11)$$

2.2. Parameter estimation of the VPM model

The VPM model has three sets of parameters to be estimated. The first parameter set is the maximum light use efficiency (ε_0) which varies with vegetation types. Information about ε_0 for individual vegetation types can be obtained from analysis of net ecosystem exchange (NEE) of CO_2 and incident PAR (μmol/m^2/s photosynthetic photon flux density) at a CO_2 eddy flux tower site. The estimation of the ε_0 parameter is largely determined by the choice of either a linear or nonlinear model between NEE and incident PAR data (generally at half-hour time-step) over a year (Frolking et al., 1998; Ruimy et al., 1995). In the VPM model, we used ε_0 value derived from the nonlinear model between NEE and PAR (Xiao et al., 2004a). For tropical evergreen forests, we used an ε_0 value of 0.045 μmol CO_2/μmol PAR, derived from the time-series data of NEE and incident PAR at the CO_2 flux tower sites (Goulden et al., in press; Malhi et al., 1998).

The second parameter set is for calculation of T_{scalar} (see Eq. (7)). For tropical forest, we used a minimum temperature (T_{min}) of 2 °C, optimum temperature (T_{opt}) of 28 °C, and maximum temperature (T_{max}) of 48 °C, as implemented in the process-based Terrestrial Ecosystem Model (Raich et al., 1991; Tian et al., 1998). The third parameter set is for calculation of W_{scalar} (see Eq. (8)). Estimation of site-specific $LSWI_{max}$ is dependent upon the optical sensor and the time series of image data. The maximum LSWI value within the plant-growing season was selected as an estimate of $LSWI_{max}$ (Xiao et al., 2004a,b).

3. The study site and data

3.1. Site-specific data from the eddy flux tower site

The field study site is an old-growth, seasonally wet tropical evergreen forest, located in the Tapajós National Forest near km67 (2°51′ S and 54°58′ W) of the Santarém-Cuiabá highway, south of Santarém, Pará, Brazil. This site (thereafter referred to as "km67 site) has an annual mean temperature of 25 °C, annual mean humidity of 85%, an annual precipitation of about 1920 mm with strong seasonal dynamics (Rice et al., in press; Saleska et al., 2003). Soils in the site are primarily nutrient-poor clay oxisols with some sandy utisols (Silver et al., 2000). The 7-month wet season is usually from December through June, and the dry season is from July to November (Fig. 1a). An eddy covariance flux tower has been operating nearly continuously at the site to measure CO_2, H_2O and energy fluxes since April 2001. A recent study (Saleska et al., 2003) reported that the forest site acted as a carbon source in the wet season and a carbon sink in the dry season, largely attributed to more ecosystem respiration (including soil respiration) in the wet season than in the dry season (Fig. 1b). High daytime NEE flux (Fig. 1b) and H_2O flux in the dry season were observed, and high GPP in the dry season were inferred (Saleska et al., 2003). These

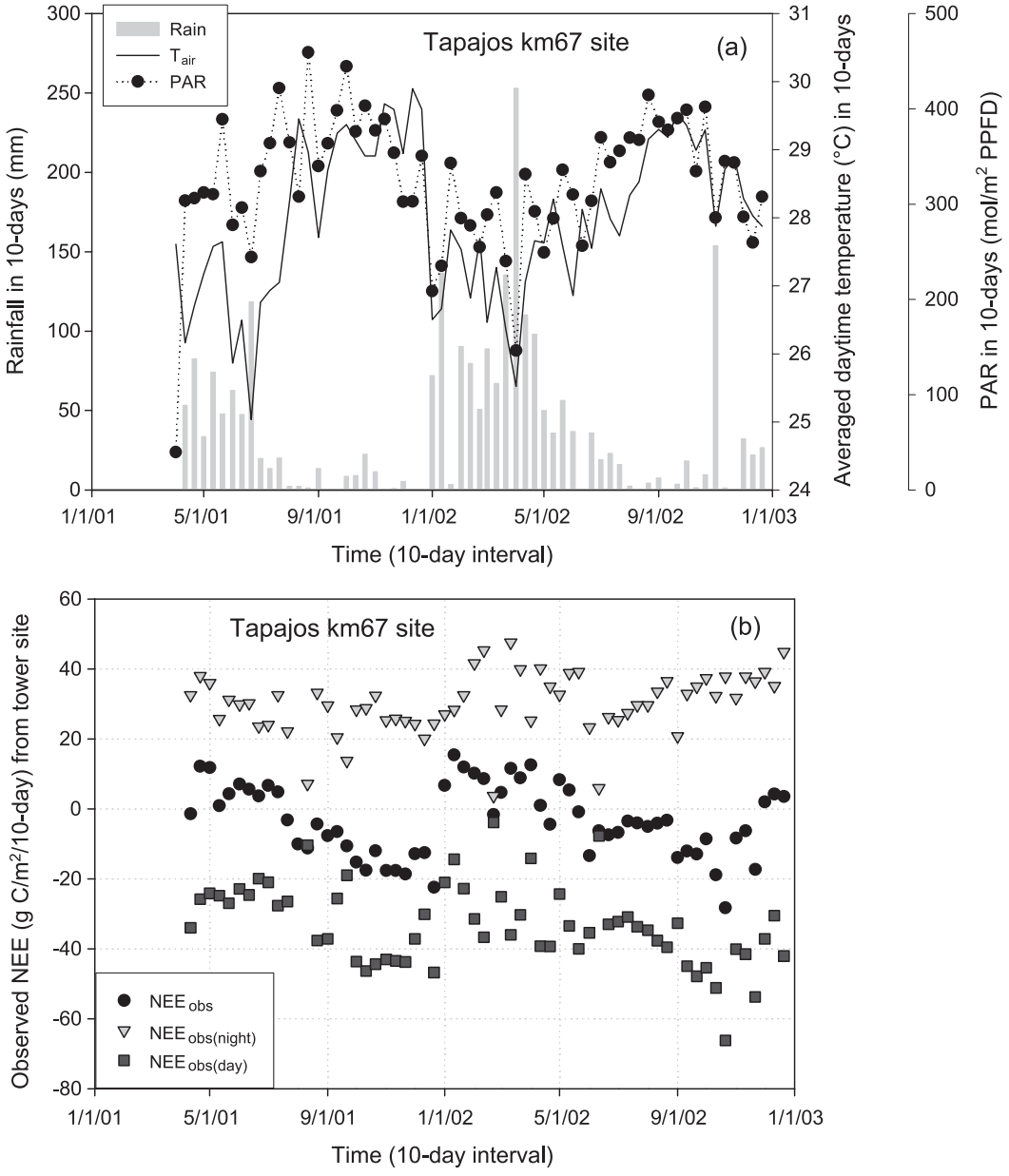

Fig. 1. The seasonal dynamics of (a) climate and (b) net ecosystem exchange of CO_2 (NEE) at the km67 eddy flux tower site in Santarém, Brazil. $NEE_{obs(night)}$—nighttime sum of NEE; $NEE_{obs(day)}$—daytime sum of NEE; NEE_{obs}—daily sum of NEE. Positive NEE values represent a carbon source and negative NEE values represent a carbon sink. The gap-filled NEE data (Saleska et al., 2003) were used in the graph and analysis.

contrast with the estimates from some process-based biogeochemical models (Botta et al., 2002; Tian et al., 1998) that predict severe soil moisture and/or water vapor pressure deficit constraints on GPP in the dry season.

Daily climate, CO_2 and H_2O flux data were aggregated to the 10-day interval as defined by the 10-day composite VGT images (see Section 3.2) and the 8-day interval as defined by the 8-day composite MODIS images (see Section 3.3), respectively. We calculated the sums of PAR and H_2O fluxes over 10- and 8-day periods, and the averages of daytime air temperature over 10- and 8-day periods. We also used the leaf litterfall data collected at the study site since July 2000 (Rice et al., in press). Litter data collection used 40 circular, mesh screen traps (0.43 m in diameter), randomly located throughout the 19.75 tree survey area. Litter samples were collected every 2 weeks. The litterfall from each trap was sorted into four categories (1) leaves, (2) fruits and flowers, (3) wood (<2-cm in diameter), and (4) miscellaneous. In this paper, we used the averaged leaf litterfall data for each of sampling periods.

3.2. 10-day composite Images from the VEGETATION sensor

The VEGETATION (VGT) sensor onboard the SPOT-4 satellite is one of a new generation of space-borne optical

sensors that were designed for the observation of vegetation and land surfaces. The VGT instrument has four spectral bands: blue (430–470 nm), red (610–680 nm), near-infrared (NIR, 780–890 nm), and shortwave infrared (SWIR, 1580–1750 nm). The blue band is primarily used for atmospheric correction. The SWIR band is sensitive to soil moisture, vegetation cover, and leaf moisture content. Unlike scanner sensors (e.g., AVHRR, MODIS), the VGT instrument uses the linear-array technology (push-broom), and thus produce high-quality images at moderate resolution (1 km) with greatly reduced distortion. Since its launch in March 1998, the VGT instrument has acquired daily images at 1-km spatial resolution for the globe.

The VEGETATION Programme produces three standard VGT products: VGT-P (physical product), VGT-S1 (daily synthesis product) and VGT-S10 (10-day synthesis product). The spectral bands in the VGT-S1 products are estimates of ground surface reflectance, as atmospheric correction of ozone, aerosols and water vapor have been applied to the VGT-P images using the Simplified Method for Atmospheric Correction (SMAC) algorithm (Rahman & Dedieu, 1994). VGT-S10 data are generated by selecting the VGT-S1 pixels that have the maximum Normalized Difference Vegetation Index (NDVI) values within a 10-day period. The maximum NDVI value composite (MVC) approach helps minimize the effects of cloud cover and variability in atmospheric optical depth. There are three 10-day composites for 1 month: day 1–10, day 11–20, and day 21 to the last day of the months. The VGT-S10 products are freely available to the public (http://free.vgt.vito.be).

We have acquired the VGT-S10 data over the period of April 1–10, 1998 to December 21–31, 2002 for the globe. We calculated NDVI, EVI and LSWI, using the surface reflectance of blue (ρ_{blue}), red (ρ_{red}), NIR (ρ_{nir}), and SWIR (ρ_{swir}) bands from the standard VGT-S10 data. A detailed description of the preprocessing and calculation of vegetation indices from the VGT-S10 data are provided elsewhere (Xiao et al., 2003). Cloudy observations in a time series of vegetation indices were gap-filled using a simple gap-filling method and the cloud quality flag in the VGT-S10 surface reflectance files (Xiao et al., 2003). In this study, we selected 3×3 pixels (approximately 3×3 km^2) that centered on the CO_2 eddy flux tower site in the Tapajós National Forest near km67 (2°51′ S and 54°58′ W) of the Santarém-Cuiabá highway, south of Santarém, Pará, Brazil (Saleska et al., 2003). We calculated the mean and standard deviation of vegetation indices over the 3×3 pixels.

3.3. 8-day composite images and 16-day composite images from MODIS sensor

Of the 36 spectral bands in the MODIS sensor, seven spectral bands are primarily designed for the study of vegetation and land surfaces: blue (459–479 nm), green (545–565 nm), red (620–670 nm), NIR (841–875 nm, 1230–1250 nm), and SWIR (1628–1652 nm, 2105–2155 nm). The MODIS sensor acquires daily images of the globe at a spatial resolution of 250 m for red and NIR (841–875 nm) bands, and at a spatial resolution of 500 m for blue, green, NIR (1230–1250 nm), and SWIR bands. The MODIS Land Science Team provides a suite of standard data products to the users (http://modis-land.gsfc.nasa.gov/), including the 8-day Surface Reflectance Product (MOD09A1) that has the above seven spectral bands at 500 m spatial resolution, and the 16-day Nadir Bidirectional reflectance distribution function (BRDF) Adjusted Reflectance (NBAR) Products (MOD43B4) that has the above seven spectral bands at 1-km spatial resolution. The MOD43B4 product provides a nadir-view reflectance in all seven bands derived from the semiempirical BRDF modeling product at the median solar zenith angle of observations over a 16-day period (Strahler & Muller, 1999). Both the MOD09A1 and MOD43B4 datasets are provided to users in a tile fashion; each tile covers 10° latitude by 10° longitude.

We downloaded the 8-day Surface Reflectance Product (MOD09A1) and the 16-day NBAR (MOD43B4) datasets for the period of 2/2000–12/2003 from the EROS Data Center, U.S. Geological Survey (http://edc.usgs.gov/). Surface reflectance values from these four spectral bands (blue, red, NIR (841–875 nm) and SWIR (1628–1652 nm)) were used to calculate the vegetation indices (NDVI, EVI, and LSWI). The procedure employed for gap-filling of cloudy pixels in the time series of vegetation indices derived from MOD09A1 was the same as that used for the VGT data set (see Section 3.2).

Based on the geo-location information (latitude and longitude) of the CO_2 flux tower site at the Tapajos km67 flux tower site, data of vegetation index data from the MOD09A1 product were extracted from 3×3 MODIS pixels (~1.5 km×1.5 km) that are centered on the flux tower. For vegetation indices from the MOD43B4 product, we only reported the data from one pixel (1-km×1-km) that is centered on the flux tower site. Simulations of the VPM model are driven by MODIS images in 2001–2002, temporally consistent with the available field data in 2001–2002.

4. Results

4.1. Biophysical performance of vegetation indices from the VGT images

We used time series data (1998–2002) of EVI and NDVI to study leaf phenology of seasonally moist tropical forest. When using the monthly precipitation threshold of <100 mm/month for definition of dry season (Saleska et al., 2003), the dry season in 2001 began in July and ended in December, and the dry season in 2002 began in June and ended in October (Fig. 1). There were distinct and consistent seasonal dynamics of EVI from 1998 to 2002 (Fig. 2a), with

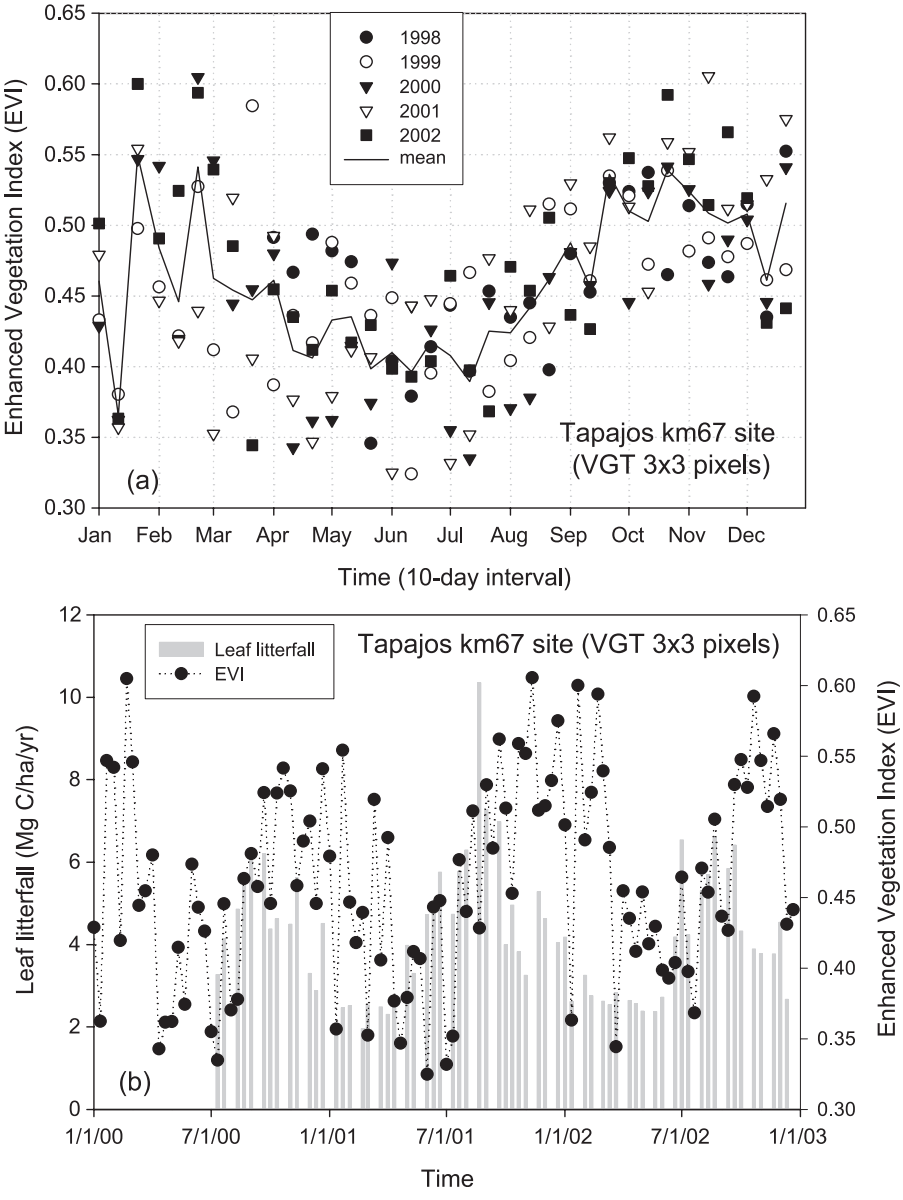

Fig. 2. The seasonal dynamics of (a) enhanced vegetation index (EVI) from 4/1998 to 12/2002, (b) EVI and leaf litterfall (Saleska et al., 2003) from 2000 to 2002 at the CO_2 eddy flux tower site in Santarém, Brazil.

low values in June–July and high values in both the late dry season (October–November) and wet season (February–March). The field data showed that leaf litterfall had a distinct seasonal dynamics in 2000–2002 (Fig. 2b). The amounts of leaf litterfall increased gradually as the dry season progressed and reached a peak in the middle of the dry season (Fig. 2b).

The plant area index (PAI) at the Tapajos National Forest varies between 5 and 7 m^2/m^2 over space and green vegetation cover is over 90% (Huete et al., 2002). The seasonal dynamics of EVI (Fig. 2a) in a year (e.g., from July 2000 to June 2001) is not likely be driven by a change in leaf area index (LAI), as the canopy of seasonally moist tropical evergreen forests has little change in LAI over seasons. It is important to note that the forest canopy is composed of mixed-age leaves. We hypothesize that the seasonal distribution of EVI in a year (Fig. 2a) may be attributed to both leaf fall of old leaves and emergence of new leaves, resulting in dynamic changes in proportions of young and old leaves within a vegetation canopy over seasons. Leaf fall of old leaves reduces self-shading, resulting in more sunlight penetrating into the canopy to the remaining younger leaves, in other words, a higher proportion of young leaves within the canopy are observed by the satellite. In general, old leaves have less chlorophyll and water content but more structural materials (e.g., lignin, cellulose), in comparison to young leaves, which could lead to significant changes in absorbance, transmittance, and reflectance of leaves as the aging processes of leaves progresses. In a field study that conducted leaf optical

measurements of a number of tropical evergreen species near Manaus in the Amazon basin (Roberts et al., 1998), NIR absorbance showed significant change, increasing from near zero for young leaves to 10% for old leaves. Canopy reflectance is largely determined by light absorption of PAV (chlorophyll) and liquid water and by light scattering of NPV. NPV proportion at the leaf scale increases as (1) the leaf ages and (2) the leaf responds to various environmental stresses (e.g., drought, O_3, fungi). Increased NIR absorbance at the leaf scale may have a larger impact at the canopy scale by dampening NIR scattering within a canopy and thereby reducing canopy reflectance (Roberts et al., 1998). Thus, removal of old leaves from the canopy (leaf litterfall) is likely to result in an increase of NIR reflectance at the canopy level. As shown in Fig. 3, NIR reflectance from the VGT 10-day composite images started to increase in July of 2001 and June of 2002, temporally consistent with the beginning of the dry season and dynamics of leaf litterfall (Fig. 3).

EVI continued to increase after leaf litterfall peaked in the middle of the dry season at the km67 site (Fig. 2a), which may be attributed to continued removal of old leaves throughout the dry season, followed by emergence (flushing) of new leaves in the late dry season. The peak EVI values had a time lag of one to 2 months after the peak leaf litterfall (Fig. 2b). Observed decreases of EVI in the mid to late wet season (March–May) could be largely attributed to the aging processes of leaves, including

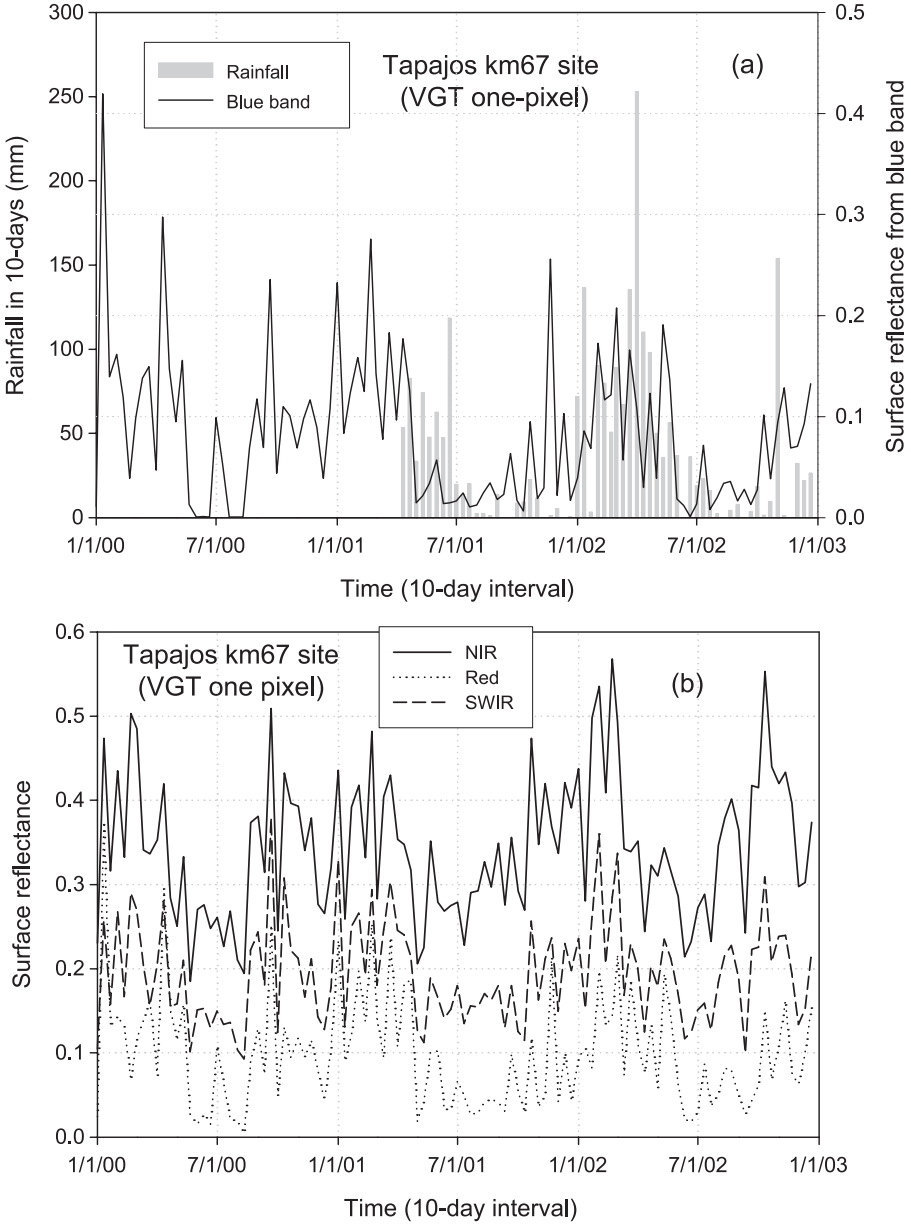

Fig. 3. The seasonal dynamics of surface reflectance values of individual spectral bands from 2000 to 2002 at the CO_2 eddy flux tower site in Santarém, Brazil. Here, we used the reflectance values from the center pixel of the 3×3 pixel block. Rainfall data from the km67 flux tower site (see Fig. 1) were also included.

increases of both leaf thickness and the nonphotosynthetic vegetation (NPV) component (e.g., veins, cell walls) within leaves. Although no seasonal field data of leaf emergence at the km67 site are available, however, field observations from other seasonal tropical forest sites suggested that many drought-tolerant species with deep roots tended to produce new leaves in the late dry season (Van Schaik et al., 1993; Wright & van Schaik, 1994). Field data at the Tapajós National Forest showed a pulse of stem growth prior to the initiation of the wet season; and increments of aboveground woody biomass (stem growth) were larger in the wet season than in the dry season (Saleska et al., 2003), which suggest that construction of new leaves may be largely done during the late part of the dry season. For the field site in Manaus, Roberts et al. (1998) reported that new leaf flush occurred mostly within the dry season. Field observations also recorded that epiphylls (fungi, lichens, algae, and bacteria) colonized the mature leaves, which affected light transmittance and absorption (Roberts et al., 1998). Relatively low EVI values in the late wet season may be attributed to both leaf age (older leaves) and epiphyll cover (Huete et al., 2003). Young leaves have a higher photosynthetic capacity than older leaves (Field, 1987), and therefore, it is essential to track changes of the age-structure of leaves in the canopy, which could substantially improve modeling of the seasonal dynamics of photosynthesis.

The NDVI time series data (1998–2002) have significantly different seasonal dynamics (Fig. 4a), in comparison to EVI. NDVI values were very low in the wet season, but

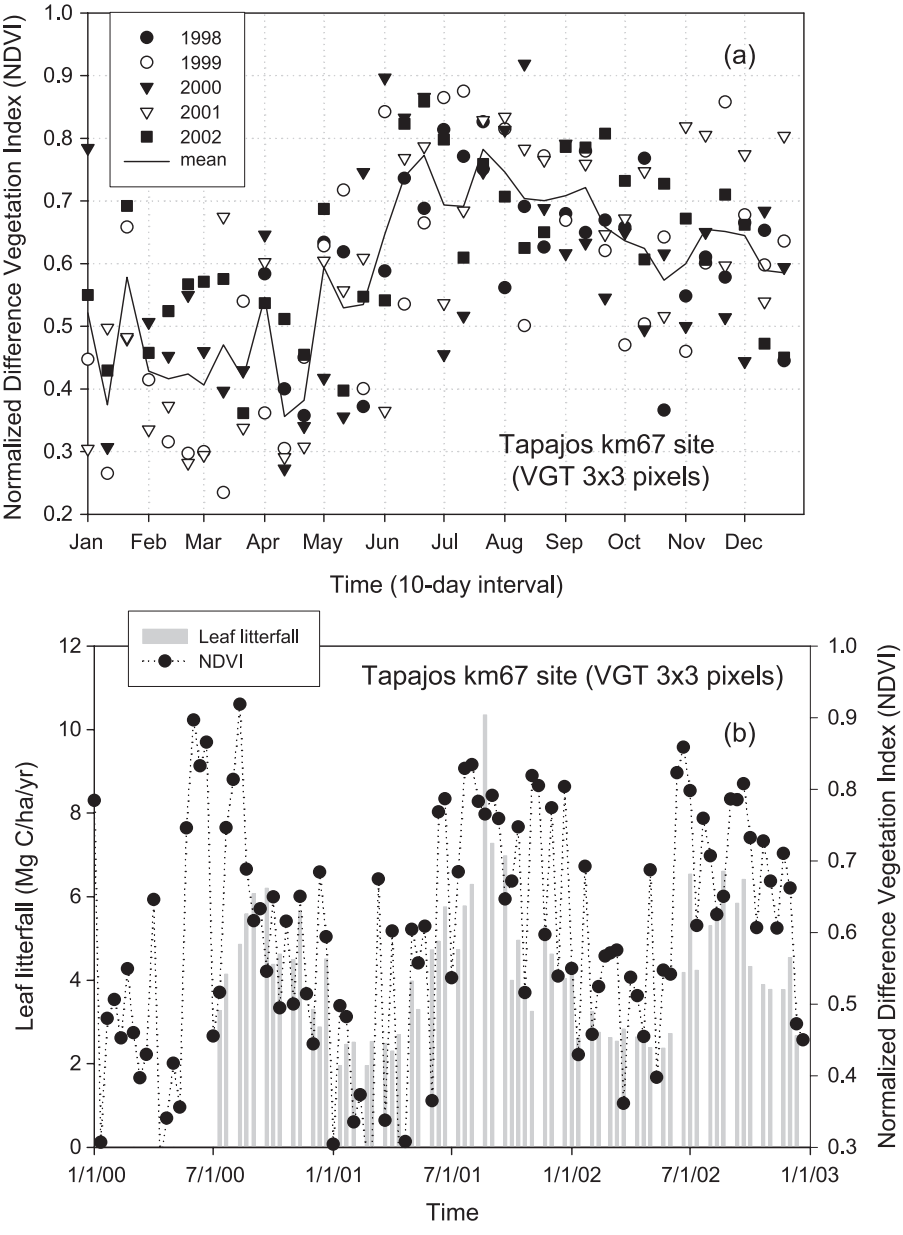

Fig. 4. The seasonal dynamics of normalized difference vegetation index (NDVI) from 4/1998 to 12/2002 at the CO_2 eddy flux tower site in Santarém, Brazil.

reached peak values in July (2001) and June (2002), much earlier than leaf litterfall reached its peak values (Fig. 4b). Low NDVI values in the wet season (January to May) were largely attributed to the effects of clouds and residual atmosphere contamination, as indicated by relatively high surface reflectance values of the red and blue bands (Fig. 3). NDVI reaches a plateau during the early part (June, July) of the dry season, largely attributed to its saturation problem associated with the mathematic formation of NDVI. After full leaf expansion, in the visible spectrum absorption dominates and reflectance values of the red band are very small. Thus, changes in the absorption of the red band have minor impacts on the calculation of NDVI. Consequently, NDVI remains a plateau level throughout the dry season (no clouds effect). The comparison between NDVI and leaf litterfall data suggests that NDVI does not reflect the subtle changes in leaf and canopy of seasonally moist tropical evergreen forests.

We used time series data (1998–2002) of LSWI to assess the status of leaf and canopy water content of the seasonally moist tropical forest over seasons. LSWI values were generally higher in the dry season than in the wet season (Fig. 5a). The seasonal dynamics of LSWI from 1999 to 2002 were negatively correlated (correlation coefficient $r=-0.56$) with that of precipitation (Fig. 5b). Soil moisture is lower in the dry season than in the wet season (Saleska et al., 2003), however, observed evapotranspiration data from the flux tower site were higher in

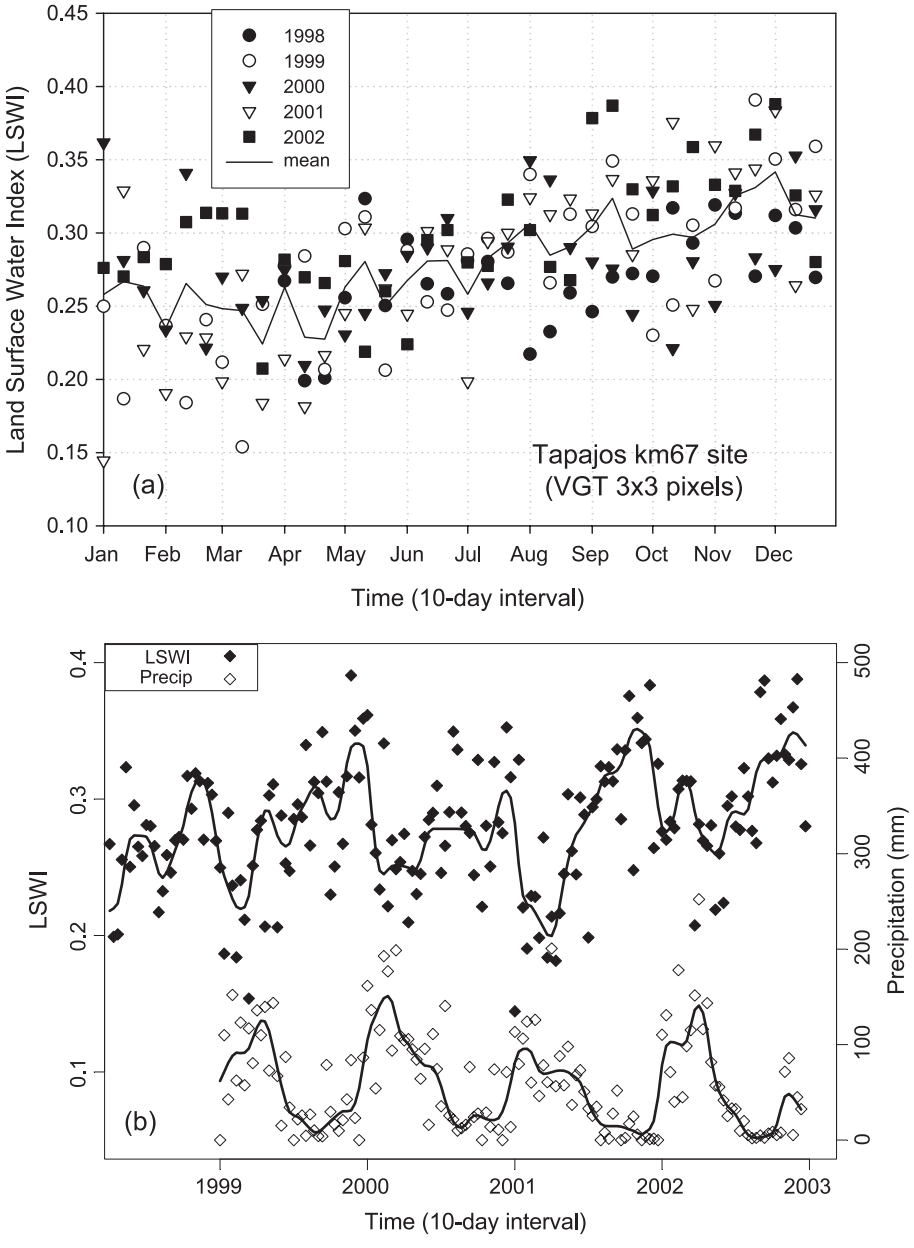

Fig. 5. The seasonal dynamics of (a) land surface water index (LSWI) and (b) precipitation, at the km67 eddy flux tower site in Santarém, Brazil. precip—precipitation (mm) from the study area (Nepstad et al., 2002).

the late dry season than in the wet season (Fig. 6a). Because of the closed forest canopy at the km67 site, soil moisture is not being measured by the VGT sensor, and it is liquid water in leaves that is being remotely sensed by the VGT sensor. High LSWI values in the dry season may be attributed to (1) high proportion of young leaves (with more leaf water content) through leaf phenology as indicated by the seasonal dynamics of EVI, and (2) higher canopy-level equivalent water thickness (EWT, g H_2O/m^2), supplied through the deep root systems. Young leaves have more water content than old leaves (Roberts et al., 1998). Further field studies are needed to measure seasonal variations in leaf water content (g H_2O/m^2) at leaf and canopy levels, although it is a technical challenge as trees in the tropical forest are very tall and thus it is difficult to collect fresh leaf samples. The seasonal dynamics of LSWI indicated that there was no water stress throughout the dry season from 4/1998 to 12/2002 at the flux tower site.

4.2. Simulation of the VPM model, using 10-day VGT composites

We ran the VPM model (Xiao et al., 2004a,b) to estimate GPP, using LSWI, EVI, and site-specific climate (air temperature and PAR) data (Fig. 1). As photosynthesis is closely coupled with H_2O flux, we use the observed H_2O flux (evapotranspiration) for the flux tower site to evaluate the performance of the VPM model. The seasonal dynamics

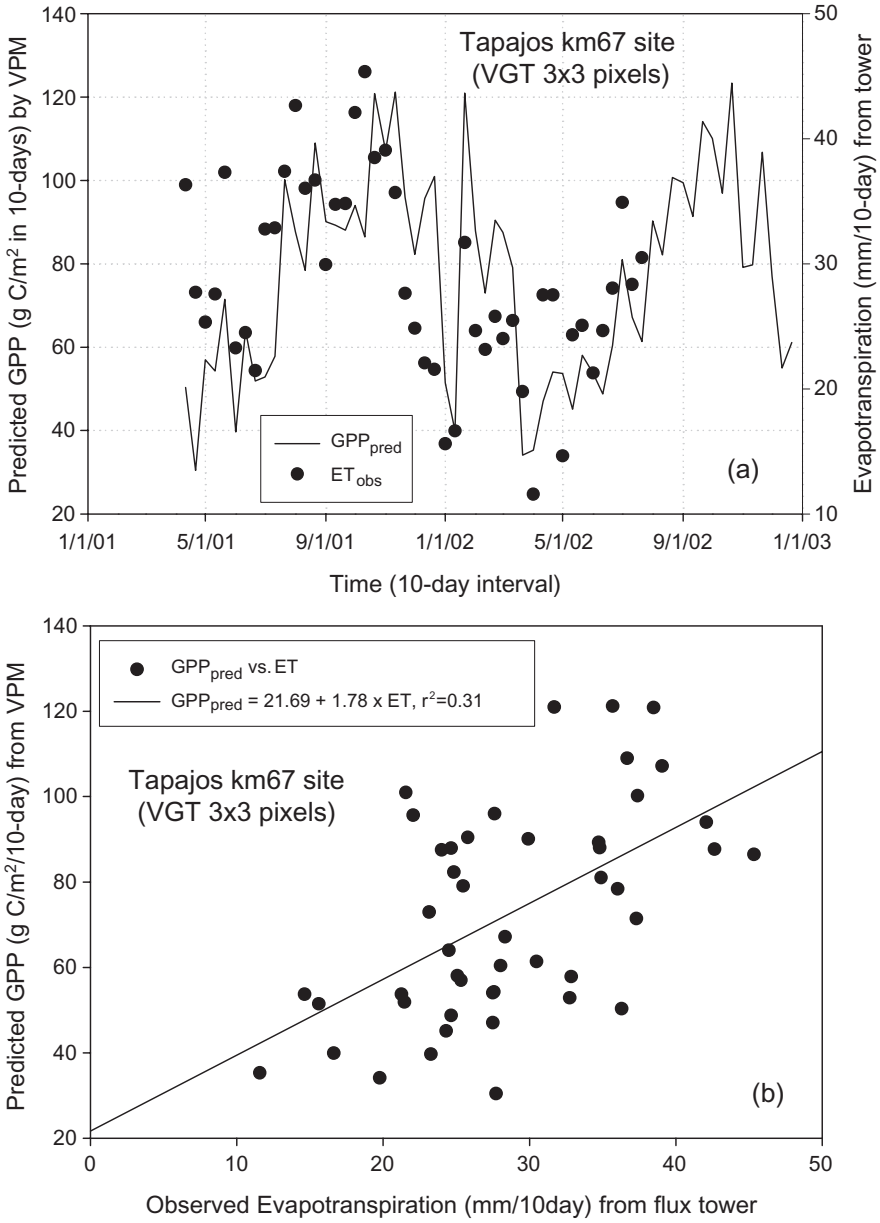

Fig. 6. The seasonal dynamics of observed evapotranspiration (ET_{obs}) and predicted gross primary production (GPP_{pred}) from the VPM model from 2001 to 2002 at the CO_2 eddy flux tower site in Santarém, Brazil.

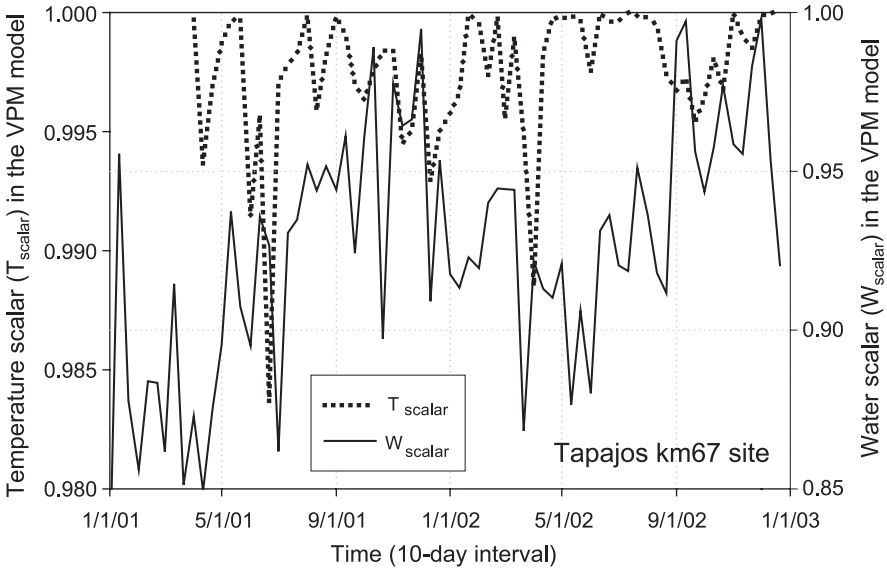

Fig. 7. The seasonal dynamics of temperature scalar (T_{scalar}) and water scalar (W_{scalar}) for the simulation of the VPM model.

of predicted GPP agreed reasonably well with that of observed evapotranspiration (Fig. 6). The VPM model predicts high GPP in the late dry season, consistent with high GPP estimates (GPP_{est}) from the eddy flux tower (Saleska et al., 2003).

GPP_{pred} values are much higher in the dry season than in the wet season, for instance, monthly GPP_{pred} was 327 g C/m^2 in October 2002 (dry season) but 162 g C/m^2 in April 2002 (wet season). The relatively low GPP_{pred} in the wet season can be attributed to a number of factors. First, there was a much smaller amount of PAR available for photosynthesis because of frequent cloud cover in the wet season (Fig. 1), for instance, monthly PAR (photosynthetic photon flux density) was 770 mole/m^2 in April 2002 but 1135 mole/m^2 in October 2002, a difference of 32%. Secondly, the averaged EVI value was lower in April 2002 (0.43) than in October 2002 (0.56) (Fig. 2), a difference of 23%. As EVI seasonal dynamics is related to leaf phenology (leaf fall, leaf emergence) at the canopy level, this suggests that leaf phenology could play an important role in the GPP calculation of seasonally moist tropical forest. Thirdly, W_{scalar} values were lower in April 2002 (0.91) than in October 2002 (0.94), a difference of 3% (Fig. 7). Temperature scalar (T_{scalar}) values varied little between April 2002

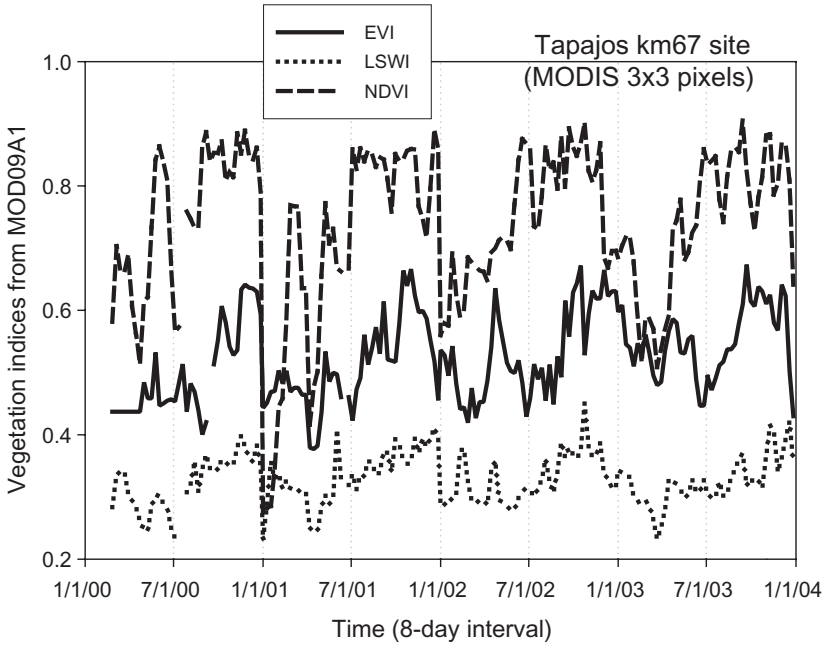

Fig. 8. The seasonal dynamics of vegetation indices derived from the 8-day MODIS Surface Reflectance Product (MOD09A1) in 2000–2003 at the CO_2 eddy flux tower site in Santarém, Brazil.

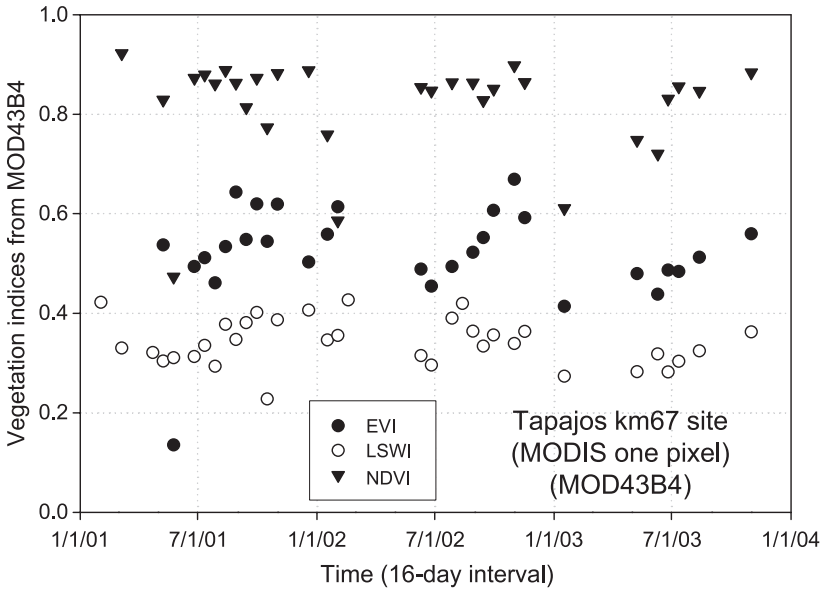

Fig. 9. The seasonal dynamics of vegetation indices derived from the 16-day MODIS Nadir BRDF-adjusted surface reflectance product (MOD43B4) in 2001–2003 at the CO_2 eddy flux tower site in Santarém, Brazil.

and October 2000 (Fig. 7). A field-based light addition/augmentation experiment for rainforest trees in Panama had suggested that light, rather than water, temperature, or leaf nitrogen, was the primary factor limiting CO_2 uptake during the rainy season (Graham et al., 2003). Annual sum of predicted GPP in 2002 for the km67 site was about 2712 g C/m^2/year, within the range from 2400 C/m^2/year at a rainforest site near Rondonia (Lloyd et al., 1995) to 3040 g C/m^2/year at a rainforest site near Manaus, Brazil (Malhi et al., 1998).

4.3. Seasonal dynamics of vegetation indices from MODIS sensor

NDVI time series data derived from the 8-day MOD09A1 product had lower values in the wet season than in the dry season (Fig. 8). NDVI reached its plateau in July of 2001 and June of 2002 (Fig. 8), similar to the NDVI time-series derived from the 10-day VGT images (Fig. 4). The seasonal dynamics of EVI derived from the 8-day MOD09A1 product (Fig. 8) was substantially different from that of NDVI. The EVI had low values in June–July but high values in late dry season, which is similar to the seasonal dynamics of EVI derived from the 10-day VGT images (Fig. 2). The seasonal dynamics of LSWI also increased gradually from the wet season to the dry season (Fig. 8).

Time series of vegetation indices derived from the 16-day MOD43B4 product had many missing data in the wet season (Fig. 9), because there were not enough numbers (7 or more) of cloud-free observations within the 16-day periods for implementing the BRDF correction algorithms. EVI time series from the 16-day MOD43B4 product had low values in June–July but high values in the late dry season (Fig. 9), which is consistent with the EVI values from the 8-day MOD09A1 product (Fig. 8).

4.4. Simulations of the VPM model, using 8-day MODIS composite images

We ran the VPM model (Xiao et al., 2004a) using the vegetation indices (Fig. 8) derived from the 8-day MOD09A1 product and site-specific air temperature and PAR data. As photosynthesis is closely coupled with H_2O flux, we use the observed H_2O flux (evapotranspiration; mm in 8-day) from the flux tower site to evaluate the performance of the VPM model. The VPM model predicts high GPP in the late dry season, consistent with high GPP estimates (GPP_{est}) derived from the eddy flux tower data (Saleska et al., 2003). The seasonal dynamics of predicted GPP agreed reasonably well with that of observed evapotranspiration (Fig. 10). The annual sum of GPP_{pred} in 2002 from the VPM model at the km67 site is about 2977 g C/m^2/year.

5. Discussion

In this study, we evaluated the seasonal dynamics of vegetation indices (EVI, LSWI and NDVI) from both the VGT sensor and the MODIS sensors for a seasonally moist tropical evergreen forest in Brazil. Strong seasonal dynamics of EVI and LSWI from the VGT and MODIS sensors were observed at the site, consistent with the observations of EVI (Huete et al., 2002, 2003). In this study, our explanations for the seasonal dynamics of EVI and LSWI focus primarily on leaf phenology, leaf age, and leaf water content. It is also important to note that a number of factors could potentially affect the calculation and seasonal

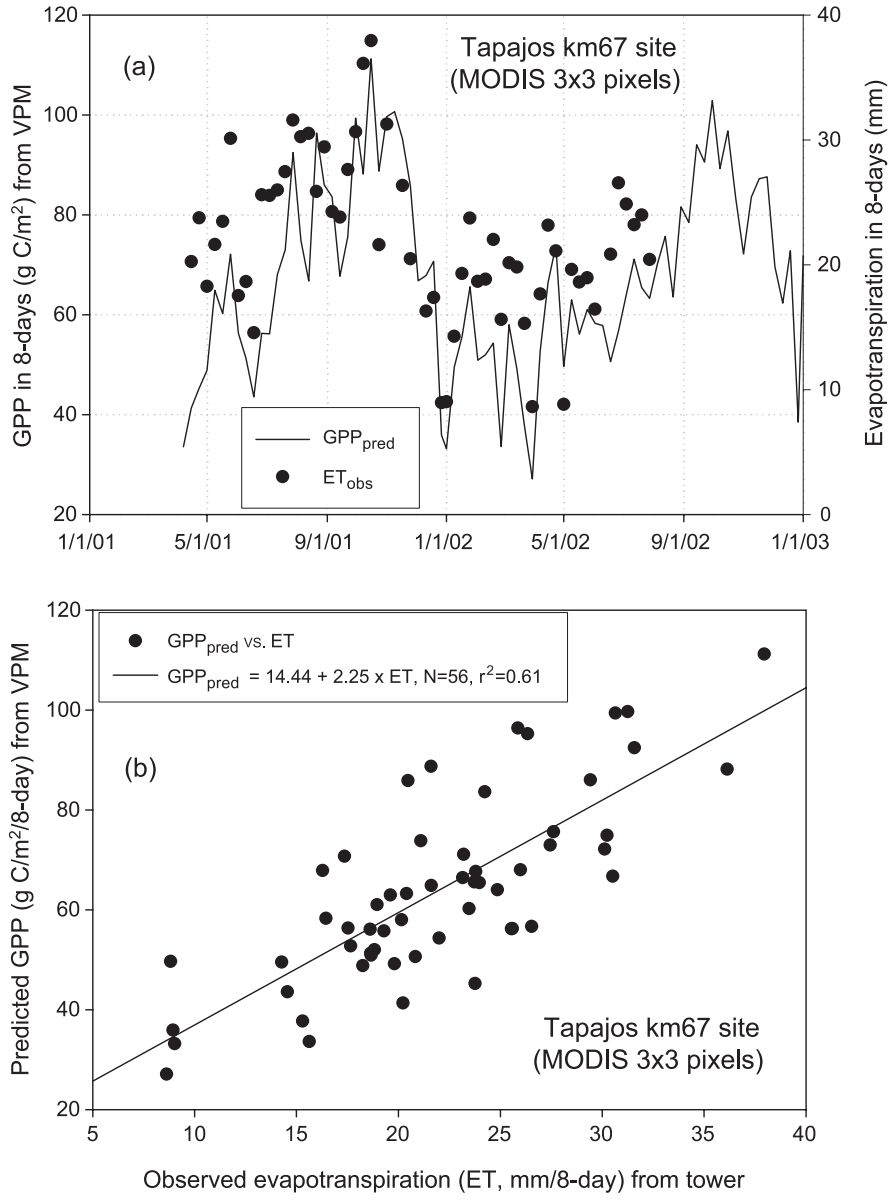

Fig. 10. The seasonal dynamics of observed evapotranspiration (ET) and predicted gross primary production from the VPM model in 2001–2002 at the CO_2 eddy flux tower site in Santarém, Brazil.

dynamics of vegetation indices, including the shadow canopy fraction within a pixel (Asner & Warner, 2003), clouds, and smoke (Huete et al., 2002; Xiao et al., 2003). Further studies are needed to quantify the relative roles of those factors on the seasonal dynamics of vegetation indices at 500-m (MODIS) to 1-km (VGT) spatial resolutions over the Amazon basin. To conduct systematic analyses of subpixel cloud cover and its impacts on vegetation indices over seasons is out of the scope of this paper because of budget and time constraint, however, here we examined a Landsat ETM+ image for illustrating the potential impact of sub-pixel cloud cover. Fig. 11 shows a color composite of Landsat 7 ETM+ image (July 30, 2001, band 5–4–3, Path–227 and Row-62) for the study area. Digital Number (DN) values of the ETM+ image were converted to reflectance, using the calibration procedure in commercial image processing software (ENVI 3.6). Vegetation indices (NDVI, LSWI, and EVI) were calculated for all the 30-m pixels of the ETM+ image. We first generated a cloud mask through unsupervised image classification (6 spectral bands at 30-m spatial resolution) and interpretation of the resultant spectral clusters. A river water body mask (at 30-m spatial resolution) was also generated and used to exclude those river water pixels from statistical analysis of vegetation indices and blue band. Then we calculated the percent fraction of cloud cover within 510-m pixels (a block of 17×17 pixels at 30-m spatial resolution), approximating to MODIS pixels at 500-m spatial resolution. Finally, we calculated the mean values of blue band reflectance, NDVI, EVI and LSWI within 510-m pixels.

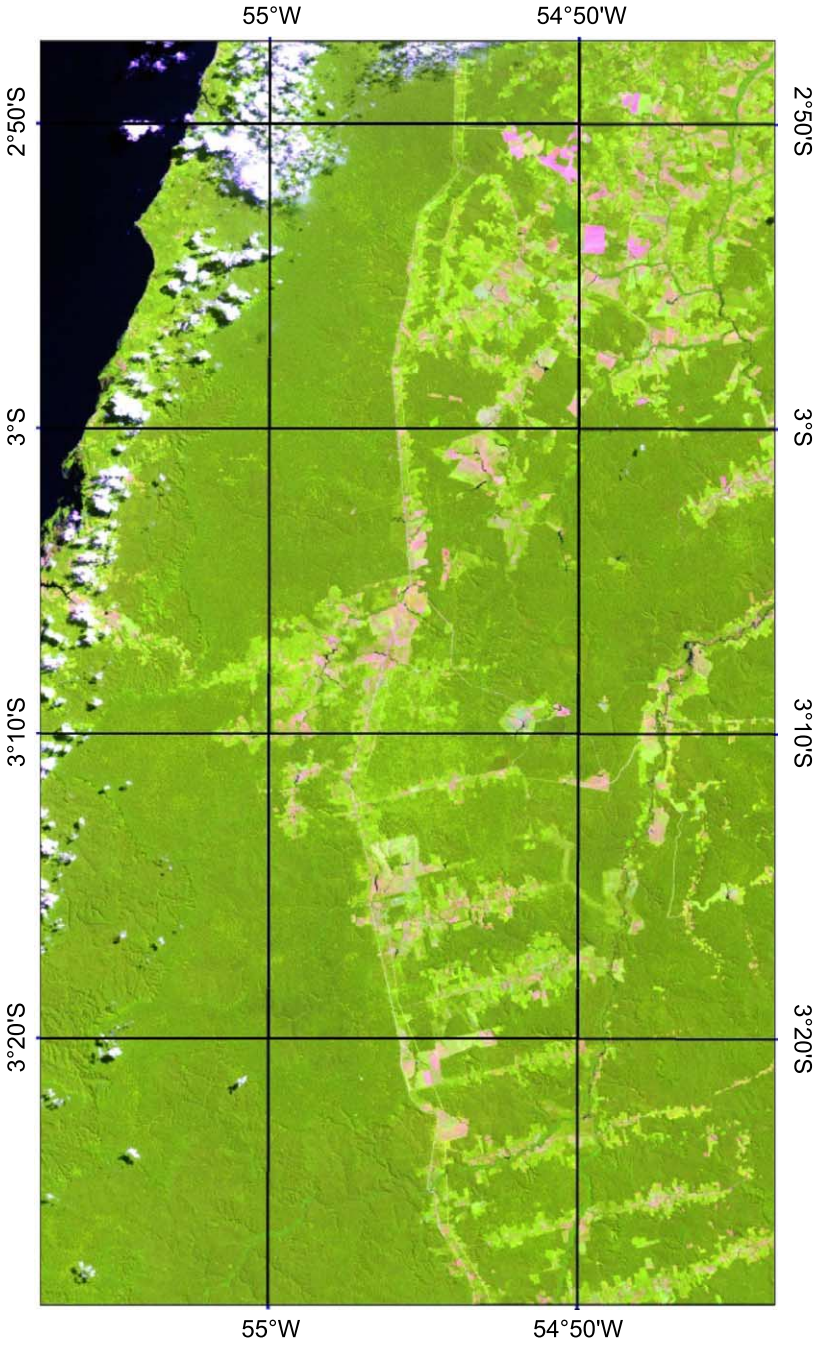

Fig. 11. The false color composite image of a Landsat 7 ETM+ image that covers the CO_2 eddy flux tower site in Santarém, Brazil (July 30, 2001; Path-227, Row-62). Three spectral bands (5–4–3, RGB) were used. (For interpretation of the references to colour in this figure legend, the reader is referred to the web version of this article).

Fig. 12 shows the relationships between percent fractions of cloud cover and reflectance of blue band and vegetation indices within 510-m pixels. Reflectance values of blue band indicate the atmospheric condition, including clouds and aerosols. Most of pixels with a blue band reflectance value of < 0.1 have a percent fraction of cloud cover below 20% (Fig. 12). When blue band reflectance value approaches 0.2 or higher, most of pixels have a percent fraction of cloud cover above 40%. Among the three vegetation indices, NDVI is most sensitive to increases of cloud cover within 510-m pixels, followed by EVI and LSWI (Fig. 12). As shown in Fig. 3a, most of observations in the dry season (July–November) had blue band reflectance values of <0.1, which suggests that the sub-pixel cloud cover, if existed during the dry season, is likely to have minor impact on vegetation indices. In other words, the dynamics of EVI and LSWI during the dry season (Figs. 2 and 5) are likely to be attributed to the leaf and canopy processes, as we described in the Results section. Only a few observations in the wet season had blue

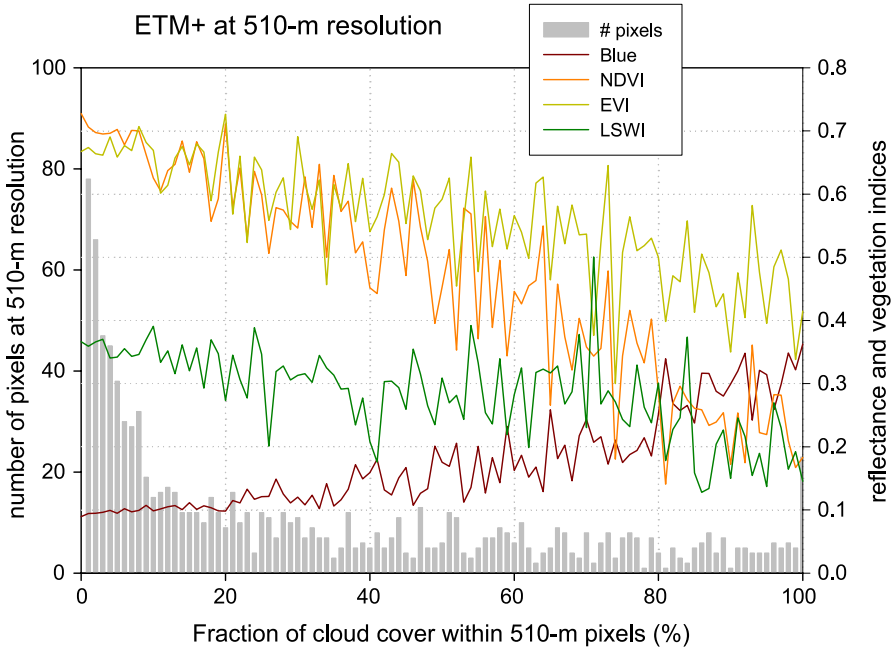

Fig. 12. The relationships between the percent fraction of cloud cover within 510-m pixels and reflectance (blue band) and vegetation indices for the study area in Santarém, Brazil (see Fig. 11 for spatial domain). EVI—enhanced vegetation index; NDVI—normalized difference vegetation index; LSWI—land surface water index. The number of pixels (11,240) with 0% fraction of cloud cover within 510-m pixels was excluded from the graph. (For interpretation of the references to colour in this figure legend, the reader is referred to the web version of this article.)

reflectance value of <0.1, which suggests that careful screening of cloud cover is needed. Future research needs to include images from both Terra (morning pass) and Aqua (afternoon pass) satellites, which together may provide more cloud-free observations (particularly in the cloudy wet season) and thus may improve our understanding of the seasonal dynamics of vegetation indices in the seasonally moist tropical forests.

In comparison to other production efficiency models (PEM) that are based on the NDVI–LAI–FAPAR relationships (Behrenfeld et al., 2001; Field et al., 1998; Nemani et al., 2003; Running et al., 2000), the VPM model implements three hypotheses and alternative approaches in its model formulation (Xiao et al., 2004a,b). The first hypothesis is the conceptual partitioning of PAV (chloroplasts) and NPV, and we assumed that advanced vegetation indices (e.g., EVI) are capable of tracking subtle changes in PAV and NPV at the leaf level, in addition to canopy-level structural changes (leaf area index, plant area index) of forests that usually has little changes over plant growing seasons. In the second hypothesis is the equivalent water thickness (EWT, g H_2O/m^2) at leaf and canopy levels, and we assume that advanced vegetation indices (e.g., LSWI) are capable of tracking changes in leaf water content over the plant growing season. In the third hypothesis is the leaf phenology (leaf fall, leaf emergence), and we assumed that improved vegetation indices (e.g., EVI and LSWI) from advanced optical sensors are capable of detecting subtle changes in leaf optical properties associated with changes in anatomical, biochemical, and biophysical properties at different leaf ages. Few studies have provided in situ seasonal measurements of leaf optical properties over plant growing seasons in the tropical forests (Roberts et al., 1998). Here we suggest that future field work should focus on seasonal measurements of leaf water content, chlorophyll, dry matter, and leaf phenology (leaf fall and emergence of new leaves) over seasons, in support of temporal analyses of advanced vegetation indices (e.g., EVI and LSWI).

The results of this study are likely to have significant implications to remote sensing analyses of seasonally moist tropical forests, the carbon cycle and climate modeling. First, the seasonal dynamics of NDVI (Fig. 4) differed significantly from that of EVI and did not reflect subtle changes in leaf phenology (leaf age), as indicated by leaf litterfall data (Fig. 4). NDVI data are closely related to LAI and have been widely used in the Production Efficiency Models that estimate GPP and NPP of forest ecosystems (Behrenfeld et al., 2001; Field et al., 1998; Nemani et al., 2003) and in the land surface parameterization (Sellers et al., 1996) for climate models. Although EVI and NDVI are complementary vegetation indices (Huete et al., 2002), the remarkable differences between EVI and NDVI seasonal patterns in seasonally moist tropical forest (Figs. 2 and 4) and temperate forests (Xiao et al., 2004a,b) call for long-term observations of leaf phenology (leaf age) and spectral measurements at the leaf and canopy levels over seasons, in conjunction with CO_2, H_2O, and energy flux measurements. In addition to measurements of canopy structure parameters (e.g., leaf area index), future field efforts should focus on measurements and analyses of anatomical, biochemical, biophysical, and physiological and optical properties of leaves over time. Our working hypothesis is that those changes associated with different leaf ages are important

factors and are likely to be tracked by advanced space-borne sensors (e.g., VGT and MODIS).

Secondly, it has been suggested that old-growth seasonally moist tropical forests have evolved two adaptive mechanisms for maintaining high photosynthesis during the late dry season. The first adaptive mechanism is the deep roots system for access to water in deep soils (Nepstad et al., 1994). The second adaptive mechanism is the leaf phenology (seasonal dynamics of leaf fall and leaf emergence) that ensures a large proportion of young foliage with high photosynthetic capacity in the canopy to utilize PAR. These hypotheses are supported indirectly by tower flux measurements (daytime NEE, evapotranspiration) and analysis of remote sensing indices (EVI, LSWI). The seasonal dynamics of predicted GPP from the satellite-based VPM model also suggested that a seasonally moist tropical evergreen forest has higher photosynthesis in the dry season than in the wet season. Information on deep root systems and leaf phenology in tropical forests are critically needed for biogeochemical, climate and hydrological, models, however, only limited field data are available on forests with deep root systems (Nepstad et al., 1994; Schenk & Jackson, 2002). Our temporal analyses of improved vegetation indices (EVI and LSWI) over seasons suggest that images from advanced optical sensors may offer a new opportunity to identify and map seasonally moist tropical forests with these two adaptive mechanisms.

Seasonal dynamics of NEE between tropical forests and atmosphere is determined by GPP and ecosystem respiration (R_e), however, to quantify the seasonal dynamics of GPP and R_e still remains a challenging task (Grace et al., 1995, 1996; Loescher et al., 2003; Saleska et al., 2003). Because these two adaptive mechanisms of seasonally moist tropical forests are not included, many process-based ecosystem models (Botta et al., 2002; Tian et al., 1998) predict low photosynthesis during the dry season, and may not accurately predict the seasonal dynamics of the carbon balance of a seasonally moist tropical forest (Saleska et al., 2003). If the majority of old-growth stands of seasonally moist tropical forest does have these two delicate and interwoven adaptive mechanisms, they may be vulnerable to very large-scale climate variability (e.g., prolonged drought, strong El Niño event), which represents a significant departure from their normal climate variability. Future efforts in the development and refinement of biogeochemical models for seasonally moist tropical forest should take these two adaptive mechanisms into consideration. CO_2 flux data from eddy flux tower sites are playing an increasing role in evaluating process- and satellite-based models (Law et al., 2000; Turner et al., 2003; Xiao et al., 2004a). In addition to CO_2 flux data, we also suggest that H_2O flux data from the eddy flux tower sites should be used for evaluating the process-based and satellite-based models, particularly in those flux sites where there were large numbers of missing CO_2 flux data in the wet season, such as the Tapajos km67 site (Saleska et al., 2003).

In summary, this study has explored the potential of improved vegetation indices (EVI, LSWI) from advanced optical sensors (e.g., VGT and MODIS) for improving seasonal characterization of leaf phenology and canopy water content of tropical evergreen forests at leaf and canopy levels. It has also demonstrated the potential of the VPM model for estimating GPP in a seasonally moist tropical evergreen forest. The VPM model can be applied at the global scale, driven by climate data and satellite images, and the resultant GPP estimates from the VPM model can be used in a diagnostic mode to constrain and improve atmospheric inversion models (Denning et al., 1995) and biogeochemical models (Botta et al., 2002; Tian et al., 1998) with prognostic capacity.

Acknowledgements

The satellite data analyses was supported by the NASA Earth Observing System Interdisciplinary Science program NAG5-10135), and Land Cover and Land Use program (NAG5-11160). The field data collection at the CO_2 eddy flux tower site in Santarém, Pará, Brazil, was supported by the NASA Large-scale Biosphere-Atmosphere Experiment in Amazon (LBA). We thank three anonymous reviewers for their comments and suggestions on the earlier versions of the manuscript.

References

Asner, G. P., & Warner, A. S. (2003). Canopy shadow in IKONOS satellite observations of tropical forests and savannas. *Remote Sensing of Environment*, *87*, 521–533.

Behrenfeld, M. J., Randerson, J. T., McClain, C. R., Feldman, G. C., Los, S. O., Tucker, C. J., et al. (2001). Biospheric primary production during an ENSO transition. *Science*, *291*, 2594–2597.

Boles, S., Xiao, X., Liu, J., Zhang, Q., Munkhutya, S., Chen, S., et al. (2004). Land cover characterization of Temperate East Asia: Using multi-temporal image data of VEGETATION sensor. *Remote Sensing of Environment*, *90*, 477–489.

Botta, A., Ramankutty, N., & Foley, J. A. (2002). Long-term variations of climate and carbon fluxes over the Amazon basin. *Geophysical Research*, 29.

Ceccato, P., Flasse, S., & Gregoire, J. M. (2002). Designing a spectral index to estimate vegetation water content from remote sensing data—Part 2. Validation and applications. *Remote Sensing of Environment*, *82*, 198–207.

Ceccato, P., Flasse, S., Tarantola, S., Jacquemoud, S., & Gregoire, J. M. (2001). Detecting vegetation leaf water content using reflectance in the optical domain. *Remote Sensing of Environment*, *77*, 22–33.

Ceccato, P., Gobron, N., Flasse, S., Pinty, B., & Tarantola, S. (2002). Designing a spectral index to estimate vegetation water content from remote sensing data: Part 1—Theoretical approach. *Remote Sensing of Environment*, *82*, 188–197.

da Rocha, H. R., Goulden, M., Miller, S. D., Menton, M., Pinto, L.D.V.O., de Freitas, H. C., et al. (2004). Seasonality of water and heat fluxes over a tropical forest in eastern Amazonia. *Ecological Applications, 14*, 522–532.

Denning, A. S., Fung, I. Y., & Randall, D. (1995). Latitudinal gradient of atmospheric CO_2 due to seasonal exchange with land biota. *Nature*, *376*, 240–243.

Field, C. (1987). Leaf-age effects on stomatal conductance. In E. Zeiger, G. Farquhar, & I. R. Cowan (Eds.), *Stomatal function* (pp. 367–384). Stanford, CA: Stanford University Press.

Field, C. B., Behrenfeld, M. J., Randerson, J. T., & Falkowski, P. (1998). Primary production of the biosphere: Integrating terrestrial and oceanic components. *Science*, *281*, 237–240.

Field, C. B., Randerson, J. T., & Malmstrom, C. M. (1995). Global net primary production-combining ecology and remote-sensing. *Remote Sensing of Environment*, *51*, 74–88.

Frolking, S. E., Bubier, J. L., Moore, T. R., Ball, T., Bellisario, L. M., Bhardwaj, A., et al. (1998). Relationship between ecosystem productivity and photosynthetically active radiation for northern peatlands. *Global Biogeochemical Cycles*, *12*, 115–126.

Goulden, M., Miller, S. D., Menton, M., da Rocha, H. R., & Freitag, H. (2004). Diel and seasonal patterns of tropical forest CO_2 exchange. *Ecological Applications, 14*, 542–554.

Grace, J., Lloyd, J., Mcintyre, J., Miranda, A., Meir, P., Miranda, H., et al. (1995). Fluxes of carbon-dioxide and water-vapor over an undisturbed tropical forest in South-West Amazonia. *Global Change Biology*, *1*, 1–12.

Grace, J., Malhi, Y., Lloyd, J., McIntyre, J., Miranda, A. C., Meir, P., et al. (1996). The use of eddy covariance to infer the net carbon dioxide uptake of Brazilian rain forest. *Global Change Biology*, *2*, 209–217.

Graham, E. A., Mulkey, S. S., Kitajima, K., Phillips, N. G., & Wright, S. J. (2003). Cloud cover limits net CO_2 uptake and growth of a rainforest tree during tropical rainy seasons. *Proceedings of the National Academy of Sciences of the United States of America*, *100*, 572–576.

Huete, A., Didan, K., Miura, T., Rodriguez, E. P., Gao, X., & Ferreira, L. G. (2002). Overview of the radiometric and biophysical performance of the MODIS vegetation indices. *Remote Sensing of Environment*, *83*, 195–213.

Huete, A., Ratana, P., Didan, K., Shimabukuro, Y., Barbosa, H., Ferreira, L. G., et al. (2003). Seasonal biophysical dynamics along an Amazon eco-climatic gradient using MODIS vegetation indices. *Anais Xi SBSR, 05–10, April* (pp. 665–672). Belo Horizonte, Brasil: Instituto Nacional de Pesquisas Espaciais.

Huete, A. R., Liu, H. Q., Batchily, K., & vanLeeuwen, W. (1997). A comparison of vegetation indices global set of TM images for EOS-MODIS. *Remote Sensing of Environment*, *59*, 440–451.

Law, B. E., Waring, R. H., Anthoni, P. M., & Aber, J. D. (2000). Measurements of gross and net ecosystem productivity and water vapour exchange of a *Pinus ponderosa* ecosystem, and an evaluation of two generalized models. *Global Change Biology*, *6*, 155–168.

Lloyd, J., Grace, A. L., Miranda, A., Meir, P., Wong, S. C., Miranda, H. S., et al. (1995). A simple calibrated model of Amazon rainforest productivity based on leaf biochemical properties. *Plant Cell and Environment*, *18*, 1129–1145.

Loescher, H. W., Oberbauer, S. F., Gholz, H. L., & Clark, D. A. (2003). Environmental controls on net ecosystem-level carbon exchange and productivity in a Central American tropical wet forest. *Global Change Biology*, *9*, 396–412.

Luizao, F. J. (1989). Litter production and mineral element input to the forest floor in a central Amazonian forest. *GeoJournal*, *19*, 407–417.

Maki, M., Ishiahra, M., & Tamura, M. (2004). Estimation of leaf water status to monitor the risk of forest fires by using remotely sensed data. *Remote Sensing of Environment*, *90*, 441–450.

Malhi, Y., Nobre, A. D., Grace, J., Kruijt, B., Pereira, M. G. P., Culf, A., et al. (1998). Carbon dioxide transfer over a Central Amazonian rain forest. *Journal of Geophysical Research-Atmospheres*, *103*, 31593–31612.

Nemani, R. R., Keeling, C. D., Hashimoto, H., Jolly, W. M., Piper, S. C., Tucker, C. J., et al. (2003). Climate-driven increases in global terrestrial net primary production from 1982 to 1999. *Science*, *300*, 1560–1563.

Nepstad, D. C., de Carvalho, C. R., Davidson, E. A., Jipp, P. H., Lefebvre, P. A., Negreiros, G. H., et al. (1994). The role of deep roots in the hydrological and carbon cycles of amazonian forests and pastures. *Nature*, *372*, 666–669.

Nepstad, D. C., Moutinho, P., Dias, M. B., Davidson, E., Cardinot, G., Markewitz, D., et al. (2002). The effects of partial throughfall exclusion on canopy processes, aboveground production, and biogeochemistry of an Amazon forest. *Journal of Geophysical Research-Atmospheres*, *107*(D(20)), 8085, doi:10.1029/2001JD000360.

Potter, C. S., Randerson, J. T., Field, C. B., Matson, P. A., Vitousek, P. M., Mooney, H. A., et al. (1993). Terrestrial ecosystem production—a process model-based on global satellite and surface data. *Global Biogeochemical Cycles*, *7*, 811–841.

Prince, S. D., & Goward, S. N. (1995). Global primary production: A remote sensing approach. *Journal of Biogeography*, *22*, 815–835.

Rahman, H., & Dedieu, G. (1994). SMAC: A simplified method for atmospheric correction of satellite measurements in the solar spectrum. *International Journal of Remote Sensing*, *15*, 123–143.

Raich, J. W., Rastetter, E. B., Melillo, J. M., Kicklighter, D. W., Steudler, P. A., Peterson, B. J., et al. (1991). Potential net primary productivity in South-America-application of a global-model. *Ecological Applications*, *1*, 399–429.

Rice, A. H., Pyle, E. H., Saleska, S. R., Hutyra, L., Palace, M., Keller, M., et al. (2004). Carbon balance and vegetation dynamics in an old-growth Amazonian forest. *Ecological Applications, 14* , 555–571.

Roberts, D. A., Nelson, B. W., Adams, J. B., & Palmer, F. (1998). Spectral changes with leaf aging in Amazon caatinga. *Trees-Structure and Function*, *12*, 315–325.

Ruimy, A., Jarvis, P. G., Baldocchi, D. D., & Saugier, B. (1995). CO_2 fluxes over plant canopies and solar radiation: A review. *Advances in Ecological*, 1–68.

Running, S. W., Thornton, P. E., Nemani, R., & Glassy, J. M. (2000). Global terrestrial gross and net primary productivity from the Earth Observing System. In O. E. Sala, R. B. Jackson, H. A. Mooney, & R. W. Howarth (Eds.), *Methods in ecosystem science* (pp. 44–57). New York: Springer Verlag.

Saleska, S. R., Miller, S. D., Matross, D. M., Goulden, M. L., Wofsy, S. C., da Rocha, H. R., et al. (2003). Carbon in amazon forests: Unexpected seasonal fluxes and disturbance-induced losses. *Science*, *302*, 1554–1557.

Sarmiento, G., Goldstein, G., & Meinzer, F. (1985). Adaptive strategies of woody species in neotropical savannas. *Biological Reviews of the Cambridge Philosophical Society*, *60*, 315–355.

Schenk, H. J., & Jackson, R. B. (2002). The global biogeography of roots. *Ecological Monographs*, *72*, 311–328.

Sellers, P., Los, S., & Tucker, C. (1996). A revised land surface parameterization (SiB2) for atmospheric GCMs: Part II. The generation of global fields of terrestrial biophysical parameters from satellite data. *Journal of Climate*, *9*, 706–737.

Silver, W. L., Neff, J., McGroddy, M., Veldkamp, E., Keller, M., & Cosme, R. (2000). Effects of soil texture on belowground carbon and nutrient storage in a lowland Amazonian forest ecosystem. *Ecosystems*, *3*, 193–209.

Strahler, A., & Muller, J. P. (1999). MODIS BRDF/Albedo products: Algorithm theoretical basis document, version 5.0. Boston University.

Tian, H. Q., Melillo, J. M., Kicklighter, D. W., McGuire, A. D., Helfrich, J. V. K., Moore, B., et al. (1998). Effect of interannual climate variability on carbon storage in Amazonian ecosystems. *Nature*, *396*, 664–667.

Turner, D. P., Ritts, W. D., Cohen, W. B., Gower, S. T., Zhao, M. S., Running, S. W., et al. (2003). Scaling Gross Primary Production (GPP) over boreal and deciduous forest landscapes in support of MODIS GPP product validation. *Remote Sensing of Environment*, *88*, 256–270.

Van Schaik, C. P., Terborgh, J. W., & Wright, S. J. (1993). The phenology of tropical forests-adaptive significance and consequences for primary consumers. *Annual Review of Ecology and Systematics*, *24*, 353–377.

Wright, S. J., & van Schaik, C. P. (1994). Light and the phenology of tropical trees. *The American Naturalist*, *143*, 192–199.

Xiao, X., Braswell, B., Zhang, Q., Boles, S., Frolking, S., & Moore, B. (2003). Sensitivity of vegetation indices to atmospheric aerosols: Continental-scale observations in Northern Asia. *Remote Sensing of Environment*, *84*, 385–392.

Xiao, X., Hollinger, D., Aber, J. D., Goltz, M., Davidson, E. A., & Zhang, Q. Y. (2004a). Satellite-based modeling of gross primary production in an evergreen needleleaf forest. *Remote Sensing of Environment*, *89*, 519–534.

Xiao, X., Zhang, Q., Braswell, B., Urbanski, S., Boles, S., Wofsy, S. C., et al. (2004b). Modeling gross primary production of a deciduous broadleaf forest using satellite images and climate data. *Remote Sensing of Environment*, *91*, 256–270.

Xiao, X. M., Boles, S., Liu, J. Y., Zhuang, D. F., & Liu, M. L. (2002). Characterization of forest types in Northeastern China, using multi-temporal SPOT-4 VEGETATION sensor data. *Remote Sensing of Environment*, *82*, 335–348.

Zhang, X. Y., Friedl, M. A., Schaaf, C. B., Strahler, A. H., Hodges, J. C. F., Gao, F., et al. (2003). Monitoring vegetation phenology using MODIS. *Remote Sensing of Environment*, *84*, 471–475.